CrossMark

An improved signal processing algorithm for VSF extraction

Xiaolin Liang[1,2] · Hao Zhang[3] · Tingting Lu[3] · Han Xiao[3] · Guangyou Fang[4] · Thomas Aaron Gulliver[5]

Abstract

Contactless detection of human beings via extracting vital sign features (VSF) is a perfect technology by employing an ultra-wideband radar. Only using Fourier transform, it is a challenging task to extract VSF in a complex environment, which can cause a lower signal to noise ratio (SNR) and significant errors due to the harmonics. This paper proposes an improved signal processing algorithm for VSF extraction via analyzing the skewness and standard deviation of the collected impulses. The discrete windowed Fourier transform technique is used to estimate the time of arrival of the pulses. The frequency of human breathing movements is obtained using an accumulation scheme in frequency domain, which can better cancel out the harmonics. The capabilities of removing clutters and improving SNR are validated compared with several well-known methods experimentally.

✉ Xiaolin Liang
iamxiaolin2016@126.com

Hao Zhang
zhanghao@ouc.edu.cn

Tingting Lu
lvtingting33@163.com

Han Xiao
hanouc@outlook.com

Guangyou Fang
gyfang@mail.ie.ac.cn

Thomas Aaron Gulliver
agullive@ece.uvic.ca

[1] Science and Technology on Electronic Test and Measurement Laboratory, The 41st Research Institute of CETC, Qingdao, China

[2] China Electronics Technology Instruments Co. Ltd, Qingdao, China

[3] Department of Electronic Engineering, Ocean University of China, Qingdao, China

[4] The Key Laboratory of Electromagnetic Radiation and Sensing Technology, Chinese Academy of Science, Beijing, China

[5] Department of Electrical Computer Engineering, University of Victoria, Victoria, Canada

1 Introduction

Non-contact detections for vital sign feature (VSF) of a living person have attracted extensive attentions from researchers worldwide in past few years (Liang 2016; Liang et al. 2018a, b; Wang et al. 2014; Singh et al. 2013). Among all these numerous detection techniques, electromagnetic detection is considered the most promising as it can extract VSF using a 2-D matrix acquired from human beings. Ultra-wide band (UWB) radars have achieved promising results like indoor target localization, human fall detection, etc. based on the continuous wave (CW) (Wang et al. 2014; Mercuri 2013; Mercuri et al. 2013; Wang 2015). As a better alternative method to the CW radars, UWB radar has been widely applied to many non-contact applications including moving targets identification (Wang et al. 2012, 2013; Koo 2013; Nijsure et al. 2013), through-wall imaging (Li et al. 2013, 2014; Hu et al. 2014), and post-earthquake search and rescue (Gu and Li 2015; Wang et al. 2018a, b; Ren 2015) due to its strong permeability and excellent range resolution. Although, many schemes have been discussed to detect VSF (Huang et al. 2010, 2016; JalaliBidgoli et al. 2016; Gennarelli et al. 2016; Le et al. 2009), these methods cannot achieve better performance especially in a complex environment and the ability to detect VSF is even unique. As a result, extensive efforts are required to apply UWB radar on detecting VSF (Vu et al. 2010; Zhuge and Yarovoy 2011; Ascione et al. 2013).

Several algorithms have been developed to detect VSF in recent years (Liu et al. 2011, 2014; Baldi et al. 2015; Li et al. 2013; Lazaro et al. 2014; Conte et al. 2010; Nezirović et al. 2010; Lv et al. 2016; Li 2013; Zhang 2013; Liang et al. 2018c, d, e, f; Wu et al. 2016; Hu and Jin 2016; Li and Lin 2008; Park et al. 2007; Naishadham and Piou 2008; Ren et al. 2016). However, most approaches are unsuitable for detecting VSF of living persons behind obstacles as they can only deal with one or some aspects like clutter removal, analysis of breath characteristics and period estimation of VSF. The fast Fourier transform (FFT) and Hilbert–Huang transform (HHT) were applied to analyse the time–frequency characteristics of VSF (Liu et al. 2011, 2014). A low complexity maximum likelihood period estimator was used to estimate the period of VSF in the additive white Gaussian noise (AWGN) conditions (Conte et al. 2010). Singular value decomposition (SVD) was employed in Nezirović et al. (2010) to detect breath signal of human beings by improving the signal to noise and clutter ratio (SNCR). The linear trend was eliminated based on linear trend subtraction (LTS) (Liang et al. 2018e). Li and Lin (2008) the complex signal demodulation was discussed to remove the unwanted noises.

In this paper, a new method is proposed to detect VSF in a complex environment. The method can better remove clutter; suppress the linear trend term and other unwanted electromagnetic noises. A novel way is proposed to acquire range estimate by employing the discrete windowed Fourier transform (DWFT) technique. We provide a whole new analytical framework to detect VSF. An improved accumulation method in frequency domain is discussed to eliminate harmonics, which makes VSF frequency accurate to obtain.

The remainder of this paper is organized as follows. In Sect. 2, the model for VSF detection is introduced. A new detection method is analyzed in Sect. 3. Section 4 shows the performance of the proposed method compared with several well-known algorithms. Section 5 summarizes the whole paper.
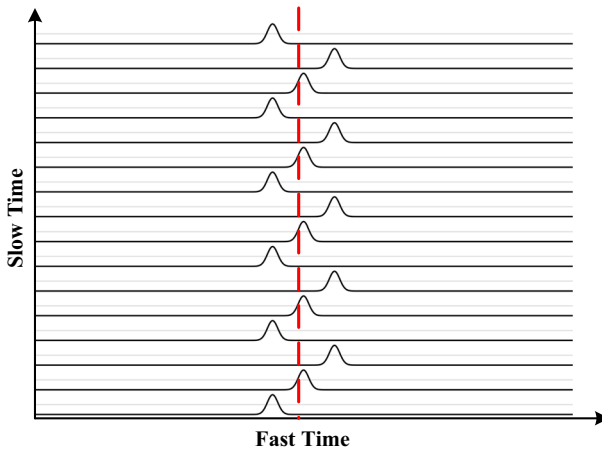
Fig. 1 The sketch map of the received pulse reflected only with breath motion

2 UWB time domain life sign model

In VSF detection, the most important is to acquire the breathing frequency of a living person. To analyze the spectrums of VSF, the time domain model is developed (Liang et al. 2018f), where slow time stands for the collected pulse number and fast time stands for the range bin. In this paper, t is the slow time and the corresponding frequency components are given by f, τ is fast time and the corresponding frequency components are given by v. Figure 1 provides the time of arrival (TOA) of the collected pulses, which can be given by (Liang et al. 2018f)

$$\widehat{\tau} = \frac{d(t)}{c} = \frac{d_0 + A_r \sin(2\pi f_r t)}{c} \tag{1}$$

where d_0 is an constant, which is used to denote the range between the human being and radar; A_r is VSF amplitude; and f_r is VSF rate.

The received pulses are

$$R(\tau) = \sum_{n=0}^{N-1} u(\tau - nT - \tau_r) * h_r(\tau)$$

$$+ \sum_{n=0}^{N-1} \sum_{p=1, p \neq r}^{P} u(\tau - nT - \tau_p) * h_p(\tau) + a(\tau) + q(\tau) + g(\tau) + \omega(\tau) \tag{2}$$

where $*$ denotes the convolution; $u(t)$ is the transmitted pulse; T is the effective pulse repetition time; t is discrete with nT, $n = 0, \ldots, N-1$; N represents the sampling points of t; $h_r(\tau)$ is the pulse response of the breathing movement; $h_p(\tau)$ is the joint pulse responses of the transmitting and receiving antenna and other static objects; $a(\tau)$ is linear trend; $w(\tau)$ is AWGN; $q(\tau)$ is non-static clutter; and $g(\tau)$ is some unwanted clutter.

Under normal breath condition, TOA can be given by

$$\tau_r = \tau_0 + \tau_r \sin(2\pi f_r nT). \tag{3}$$

where $\tau_0 = 2d_0 / v$, and $\tau_r = 2A_r / v$.
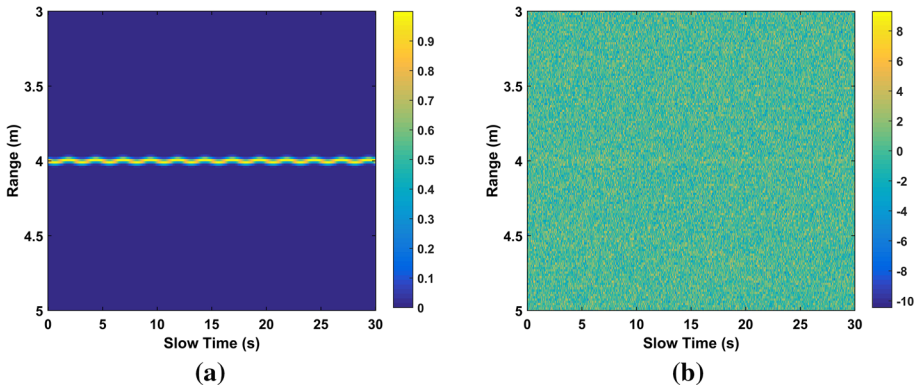
Fig. 2 The results **a** without clutter, and **b** under AWGN

Assuming that τ is discrete with δ_T, $\delta_R = \upsilon\delta_T / 2$ is the sampling interval in range. The discrete signal can be expressed as a 2-D matrix $\mathbf{R}_{M \times N}$

$$\mathbf{R} = \mathbf{h} + \mathbf{c} + \mathbf{a} + \mathbf{w} + \mathbf{q} + \mathbf{g} \tag{4}$$

where $m = 0, \ldots, M - 1$ is the sampling points of τ.

As shown in (2), there are various clutters in a complex environment, which make it challenging to extract VSF. Figure 2a shows the ideal signal only with breath motion, while the signal under AWGN is given in Fig. 2b.

3 VSF detection algorithm

In this section, the implementation steps of VSF detection are discussed as shown in Fig. 3.

3.1 Pre-processing step

VSF of a living person is usually covered by $\mathbf{c}$ with strong amplitudes, which is estimated as (Liang et al. 2018a)

$$\Im = \frac{1}{M \times N} \sum_{m=1}^{M} \sum_{n=1}^{N} R[m, n]. \tag{5}$$

The results via suppressing $\mathbf{c}$ is given by

$$\boldsymbol{\Omega} = \mathbf{R} - \Im. \tag{6}$$

LTS method is used to remove $\mathbf{a}$ (Liang et al. 2018b)

$$\mathbf{W} = \boldsymbol{\Omega}^{\mathrm{T}} - \mathbf{X}(\mathbf{X}^{\mathrm{T}}\mathbf{X})^{-1}\mathbf{X}^{\mathrm{T}}\boldsymbol{\Omega}^{\mathrm{T}} \tag{7}$$

where $\mathbf{X} = [\mathbf{x}_1, \ \mathbf{x}_2]$, $\mathbf{x}_1 = [0, \ 1, \ \ldots, \ N - 1]^{\mathrm{T}}$, and $\mathbf{x}_2 = [1, \ 1, \ \ldots, 1]^{\mathrm{T}}_{N \times 1}$.

An infinite impulse response band-pass filter is performed on (7) to enhance SNR, which is given by (Liang et al. 2018e)

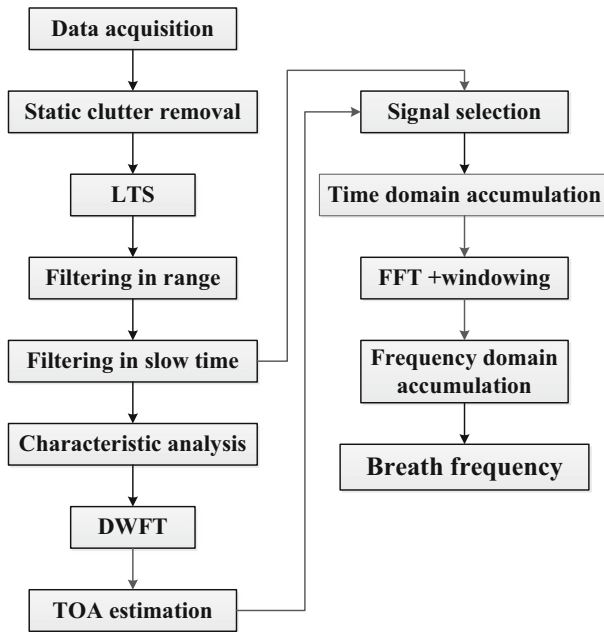$$\boldsymbol{\Lambda} = \alpha\mathbf{W} - \beta\mathbf{W} \tag{8}$$

Fig. 3 The proposed detection method

where the coefficients $\boldsymbol{\alpha}$ and $\boldsymbol{\beta}$ can be acquired automatically (Liang et al. 2018d).

And another filter with seven values averaged is developed to enhance VSF amplitude, which is given by (Liang et al. 2018f)

$$\mho[k, n] = \sum_{m=7\times k}^{7\times k+6} \Lambda[m, n] \Big/ 7 \tag{9}$$

where $k = 1, \ldots, \lfloor M/7 \rfloor$, $\lfloor M/7 \rfloor$ is the maximum integer less than $M/7$.

3.2 TOA estimation

This section provides a novel scheme for TOA estimate via analyzing the characteristics including the skewness (S) and standard deviation (SD) of VSF in (9). S is (Liang et al. 2017)

$$S_m = \mathrm{E}\Big[\big((\mho_m - \mu)\big/6\big)^3\Big] \tag{10}$$

where $\mathrm{E}[\cdot]$ is the expectation, μ and σ are mean value and deviation, respectively.

SD is given by

$$SD_m = \sqrt{\left(\sum_{n=1}^{N} (\mho_m - \mu)^2\right)\Big/ N - 1}. \tag{11}$$

To achieve TOA estimate, the SD-based S spectral i.e. SDS are calculated using (10) and (11). Figure 4 provides SDS values **Z** using a dataset acquired from one volunteer at 600 cm outdoors, which follow periodicity in target area approximately. DWFT is applied to obtain

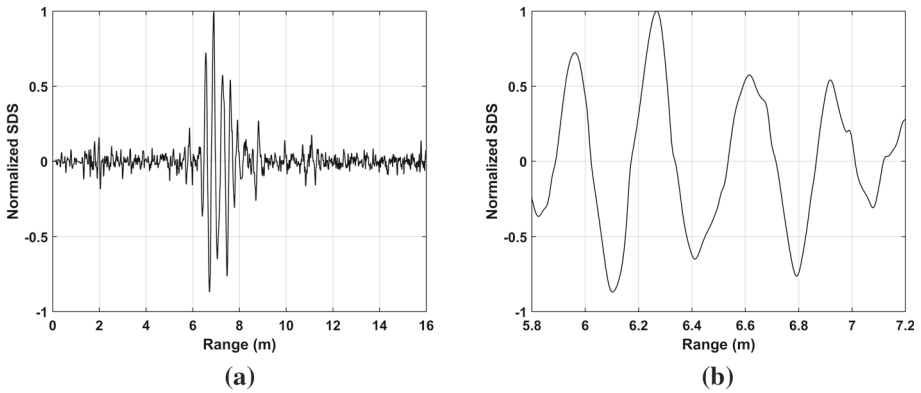**Fig. 4** **a** SDS values with the normalized amplitude, and **b** SDS in target area
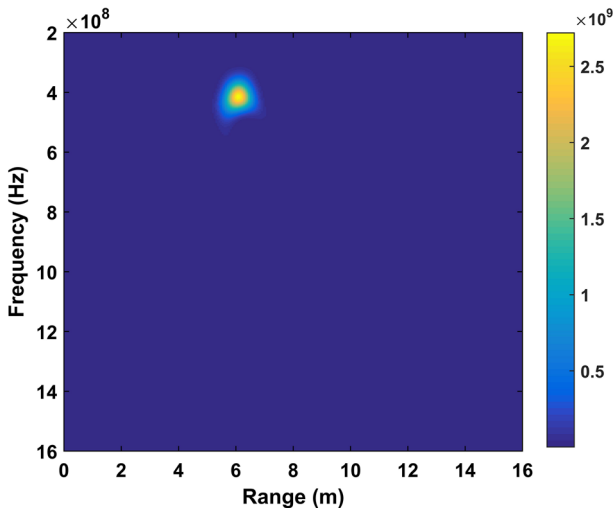

Fig. 5 The time–frequency matrix using DWFT

TOA estimate via analyzing the time–frequency characteristics as shown in Fig. 5 (Allen 1977; Wójcicki et al. 2008), which is expressed as

$$K[o, p] = \sum_{m=1}^{M} \mathbf{Z}_m \, \Xi[o - m] e^{-j2p\pi m/P}. \tag{12}$$

where p is the pth frequency component in P discrete components, and Ξ is used Hamming function with the length $O = 512$ (Mak et al. 2016) given by

$$\Xi(o) = 0.54 - 0.46 \times \cos\left(\frac{2\pi o}{512}\right), \quad o = 0, 1, \dots, 512. \tag{13}$$

The range is estimated as

$$\widehat{L} = v\widehat{\tau} \tag{14}$$

where TOA estimate $\widehat{\tau}$ corresponds to the maximal **K**.

3.3 Frequency estimation

The $\widehat{\tau}$ index in $\mho$ is

$$\Im = \widehat{\tau} / \delta_T. \tag{15}$$

To estimate VSF frequency, the accumulation method in time domain is first applied to reduce harmonics, which is given by

$$\widetilde{O}[i] = \sum_{i=\Im-50}^{\Im} |\mho_i|^2. \tag{16}$$

Usually, VSF frequency is within 0.2–0.4 Hz (Marple 1999). To improve SNR, the frequency components outside these frequencies are removed by employing a rectangular window $\boldsymbol{\theta}$ within 0.1–0.8 Hz, which is given by

$$\boldsymbol{\pi} = \boldsymbol{\theta} \odot \{FT\{\widetilde{\mathbf{O}}\}\}. \tag{17}$$

VSF frequency can be acquired as

$$\widetilde{f} = \mathbf{w}(\gamma) \tag{18}$$

where γ corresponds to the index of the maximal (17).

And the accumulation method in frequency domain is used to cancel out harmonics (Marple 1999), which is given by

$$H(\omega) = \begin{cases} 2\pi(\omega), & \omega > 0 \\ \pi(\omega), & \omega = 0 \\ 0, & \omega < 0 \end{cases}. \tag{19}$$

4 Data acquisition

4.1 UWB radar

The UWB radar prototype used to acquire the pulses is operated by employing a wireless personal digital assistant. Table 1 provides the key parameters. Using the radar system, M = 4096 sampling points are obtained in range direction. The SNR is improved by averaging every 128 collected pulses. The pulses are saved every 0.1092 s, which is acquired from $128 \times 512/600{,}000$. A joint sampling technique is developed in the receiver based on the equivalent-time and real-time sampling methods, which outperforms the analogue receiver with only one method. Figure 6 shows the pulses with the normalized amplitude.

4.2 Measurement setup

To survey the performance of the presented method, two experiments on human beings are carried out indoors and outdoors, respectively. Figure 7a shows a setup considered to acquire data. In these experiments, the radar is on a desk 1.5 m in height, and these volunteers breathed normally, kept stationary, and faced radar. In the first experiment, one girl served as the volunteer as given in Fig. 7b. This experiment is carried out outdoors. The range between the receiver and the volunteer is 300 cm, 600 cm, 900 cm, and 1100 cm, respectively. The wall is composed of three materials like brick (30 cm), reinforced concrete (35 cm) and plank

Table 1 The key parameters for the used radar	Parameters	Value
	Center frequency	400 MHz
	Amplitude of transmitted signal	50 V
	Pulse repeated frequency	600 kHz
	Average number	128
	Total time window	81 ns
	Sampling points	4096
	Antenna gain	5–7 dBi
	Input bandwidth of ADC	2.3 GHz
	ADC sampling rate	500 MHz
	Data bit	12 bit
	Dynamic range of receiver	72 dB
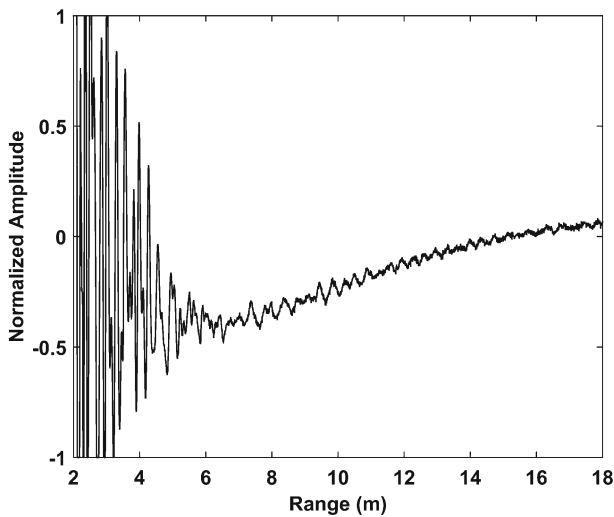
Fig. 6 The normalized pulse using UWB radar

(35 cm). The second experiment is conducted indoors with one boy served as the volunteer as shown in Fig. 7c. The range between the receiver and the volunteer is 400 cm, 700 cm, 1000 cm, and 1200 cm, respectively. Four algorithms including the FFT, HOC, constant false alarm ratio (CFAR), and advance method (AM) are used for data analysis.

5 Results and discussions

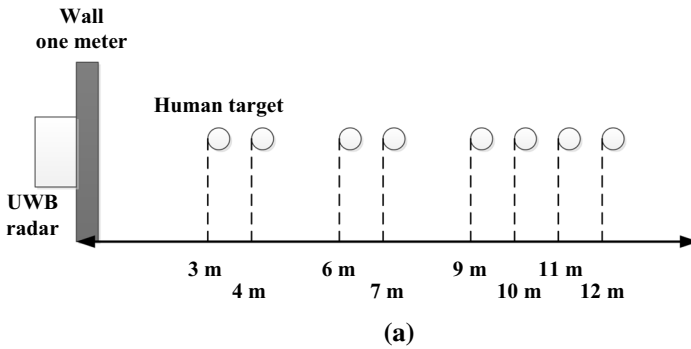In this section, the progress of the presented method is clarified in different aspects.

(a)

(b)   **(c)**

Fig. 7 a The setup for data acquisition, **b** outdoors environment, and **c** indoors environment

5.1 Intuitive detection performance

The results of pre-processing steps are given in Fig. 8 based on the pulses acquired outdoors at 900 cm. Figure 8a shows the received VSF signals. Results indicate VSF is invisible due to the influences of various clutters. The range-slow time matrix by removing clutter is given in Fig. 8b. Figure 8c shows the results by employing LTS method. Results show VSF is too weak to extract. Figure 8d shows the acquired matrix by employing a band-pass filter, and Fig. 8e shows the matrix based on the averaging filter. After the pre-processing steps mentioned above, the clutters are removed and VSF is improved comparing with the pulses as shown in Fig. 8a.

5.2 SNR improvement capability

Usually, the Cramer–Rao low bound of the unbiased VSF frequency increases as SNR increase. VSF can be extracted accurately by improving SNR, which is given by (Liang et al. 2018f)

$$\text{SNR} = 20 \cdot \log_{10}\left(\frac{\sum_{n=\mu_r-1}^{\mu_r+1} |\delta[n]|}{\sum_{n=\gamma_1}^{\mu_r-2} |\delta[n]| + \sum_{n=\mu_r+2}^{\gamma_2} |\delta[n]|}\right), \quad (20)$$

where μ_r is VSF frequency estimate, γ_1 and γ_2 are the boundaries of the adopted window.

The ability to improve SNR can be evaluated qualitatively using the data acquired at different distances. Figure 9 shows **Z** with normalized amplitudes based on the collected pulses outdoors. As shown in Fig. 10, the range estimates are 3.079 m, 6.113 m, 9.084 m and
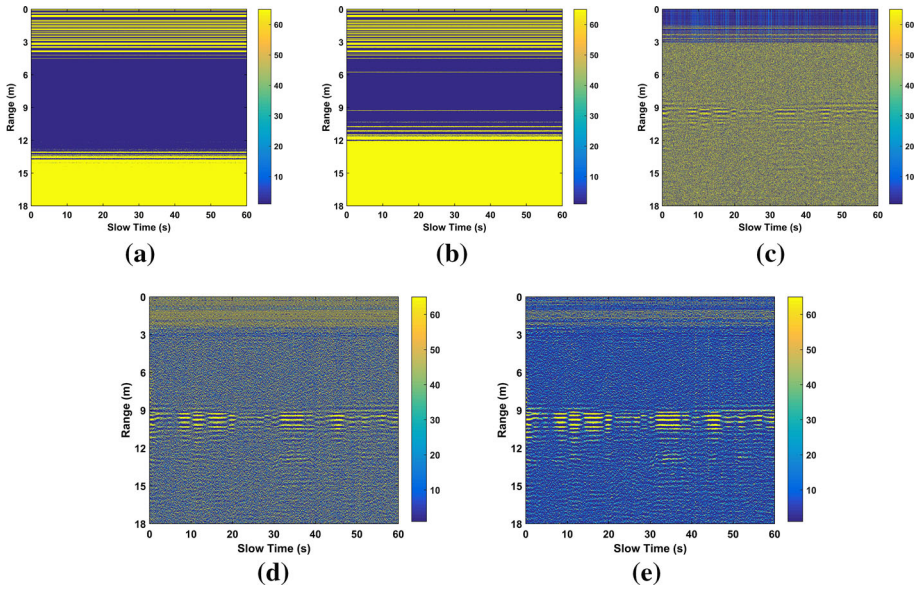
Fig. 8 The range-slow time matrix of **a** received signal, **b** clutter removal, **c** LTS, **d** band-pass filter, and **e** filtering in slow time
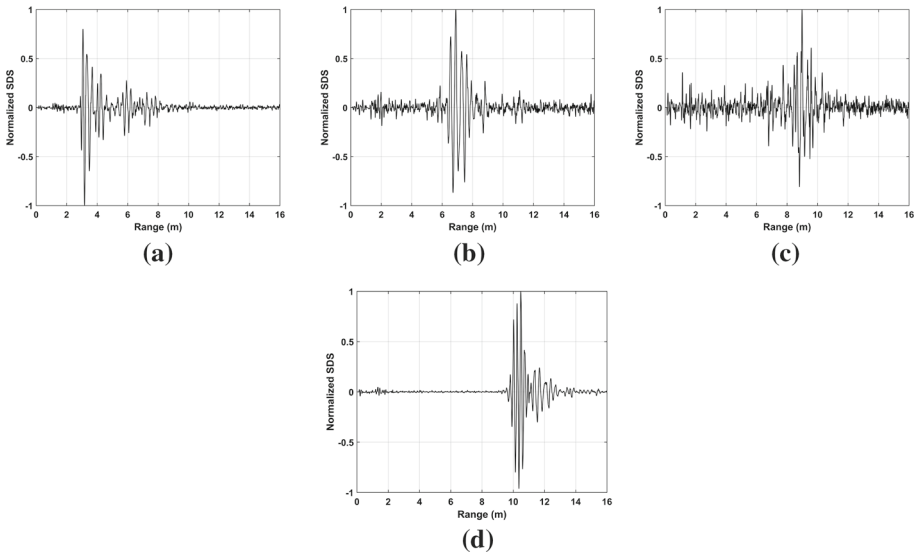
Fig. 9 The SDS values at **a** 3 m, **b** 6 m, **c** 9 m, and **d** 11 m from the receiver

11.24 m with the errors 0.079 m, 0.113 m, 0.084 m and 0.24 m, respectively. VSF frequency estimations are respectively 0.2308 Hz, 0.2307 Hz, 0.2932 Hz and 0.3329 Hz as shown in Fig. 11. The range and frequency estimations based on AM are given in Fig. 12. The ranges are 3.942 m, 6.86 m, 3.837 m and 18.58 m, and VSF frequencies are 0.087 Hz, 0.2038 Hz,
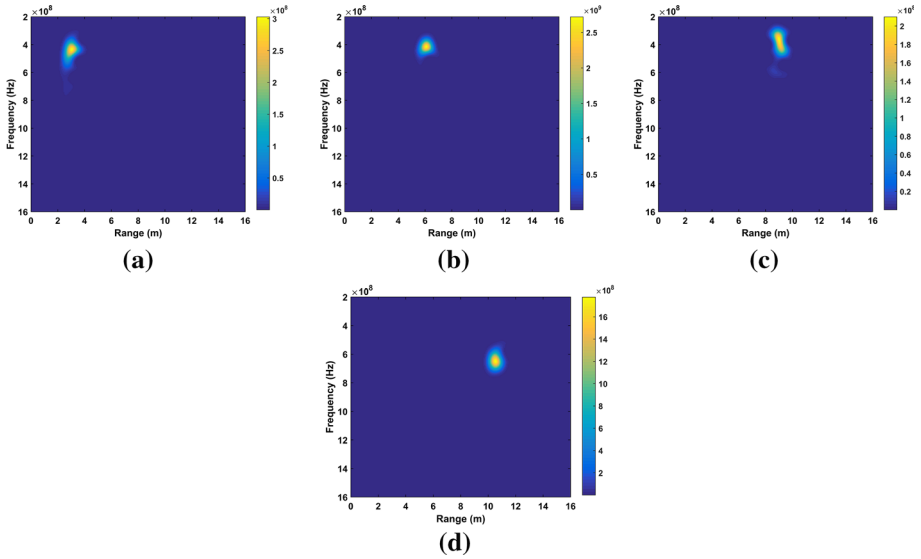
Fig. 10 Range estimations at **a** 3 m, **b** 6 m, **c** 9 m, and **d** 11 m from the receiver
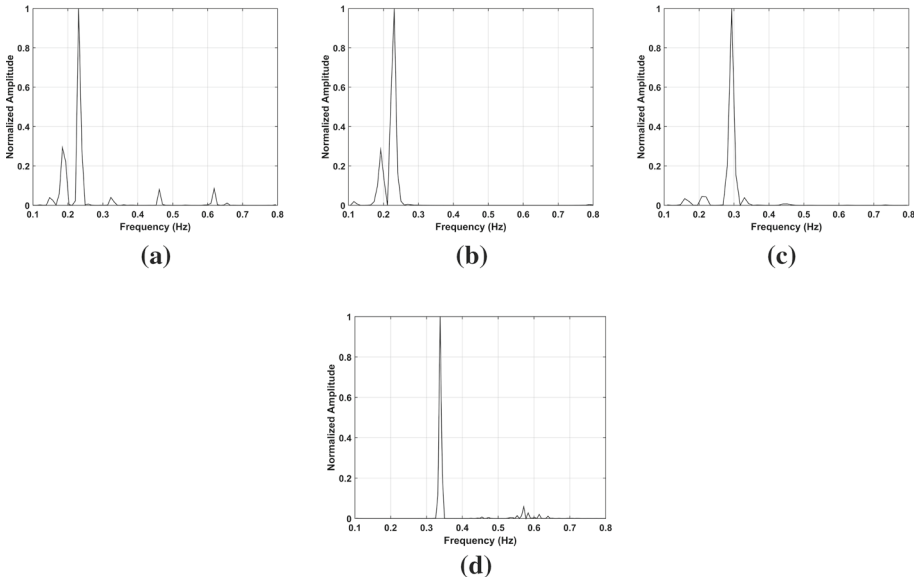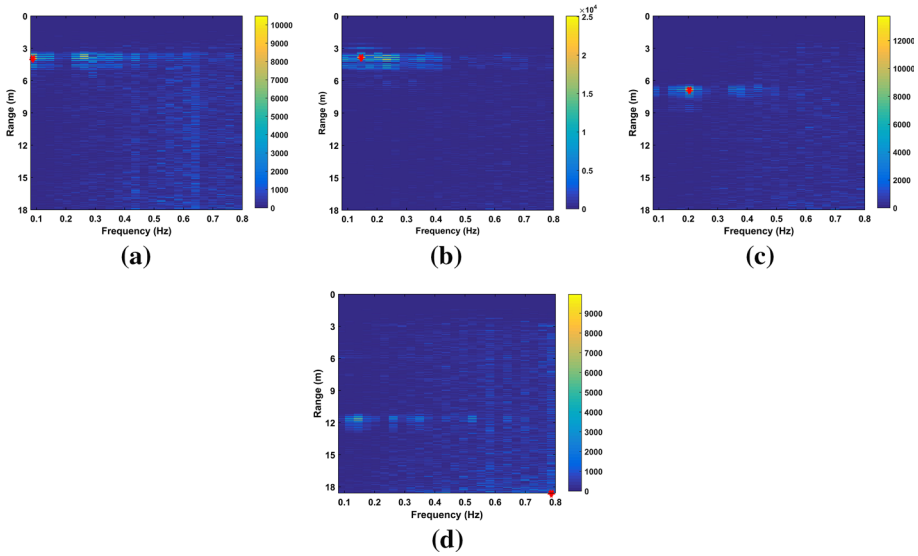

Fig. 11 Breath frequency estimations at **a** 3 m, **b** 6 m, **c** 9 m, and **d** 11 m from the receiver

0.1456 Hz and 0.7862 Hz, respectively. AM can only detect VSF in short-range. Table 2 gives comparison results based on different methods. It can be seen that the presented algorithm outperform AM in accuracy and SNR improvement.

Fig. 12 Life signal estimations using AM at **a** 3 m, **b** 6 m, **c** 9 m, and **d** 11 m from the receiver

Table 2 Performance with different methods

Method	Estimate	300 cm	600 cm	900 cm	1100 cm
Proposed	Range (m)	3.079	6.113	9.084	11.24
	Frequency (Hz)	0.2308	0.2307	0.2932	0.3329
	SNR (dB)	5.62	4.82	2.17	2.12
AM	Range (m)	3.942	6.86	3.837	18.58
	Frequency (Hz)	0.087	0.2038	0.1456	0.7862
	SNR (dB)	2.78	− 5.04	− 14.29	− 15.64

5.3 Indoors performance

In this section, the data acquired indoors are used to evaluate the detection performance at different distances. Figure 13 shows **Z** with the normalized amplitudes. The calculated ranges based on the presented algorithm are given in Fig. 14. They are respectively 4.122 m, 7.078 m, 10.071 m and 12.25 m. Figure 15 shows VSF frequencies 0.2469 Hz, 0.238 Hz, 0.2221 Hz and 0.2701 Hz, respectively.

5.4 Clutter removing capability

In this section, the capability of clutter removal is analyzed based on the data acquired at 900 cm outdoors. Figure 16 shows the calculated spectrums by employing different detection algorithms. The results using FFT are given in Fig. 16a. Various clutters exist in the effective band of breath motion, which makes it challenging to extract VSF. The results with the accu-
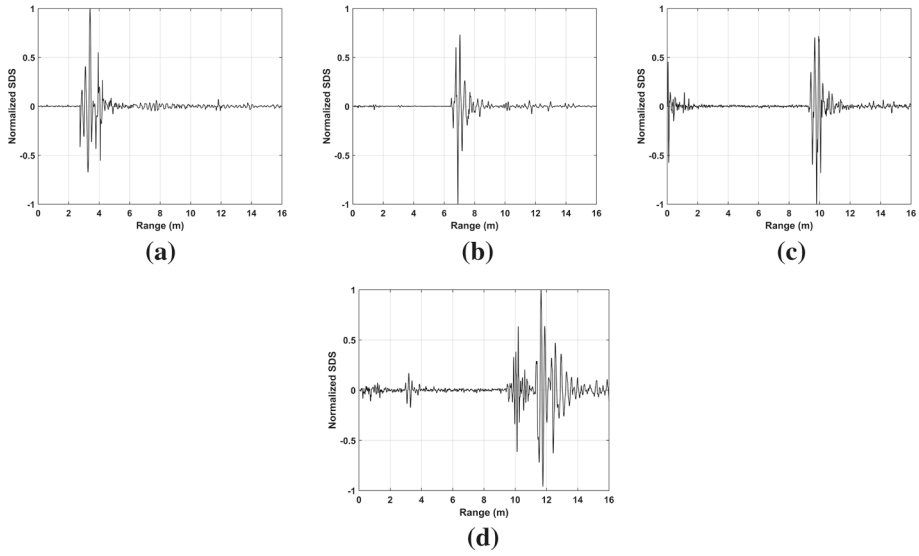
Fig. 13 SDS values at **a** 4 m, **b** 7 m, **c** 10 m, and **d** 12 m from the receiver
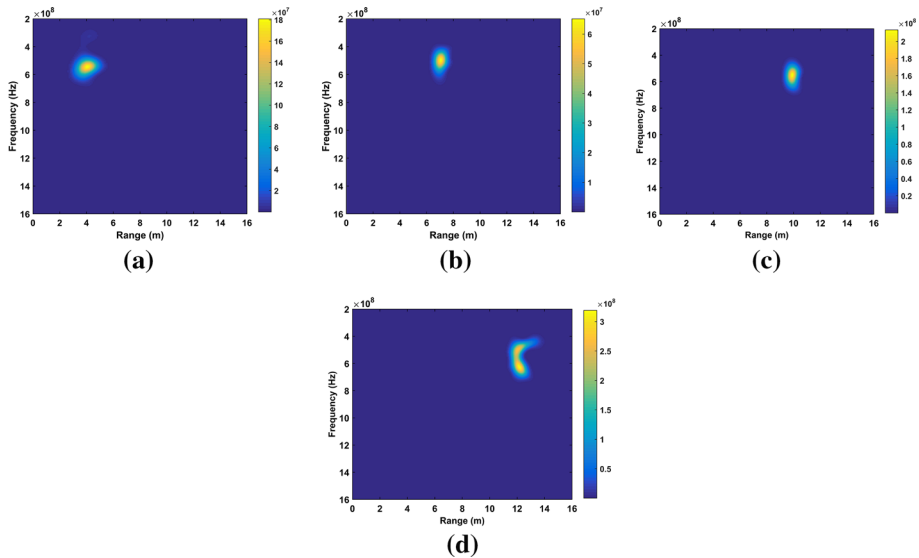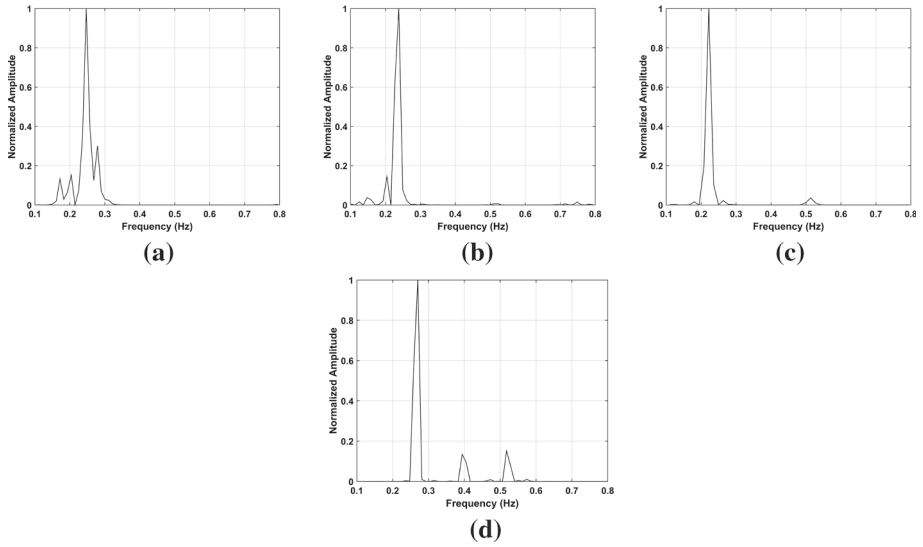

Fig. 14 Range estimations at **a** 4 m, **b** 7 m, **c** 10 m, and **d** 12 m from the receiver

mulation method in frequency domain performed different times are shown in Fig. 16b–e. Results indicate the harmonics and mixed products of life signal can be cancelled out effectively when HHT is performed four times known as four FA compared with other times as given in Table 3.

Fig. 15 Frequency estimations at **a** 4 m, **b** 7 m, **c** 10 m, and **d** 12 m from the receiver
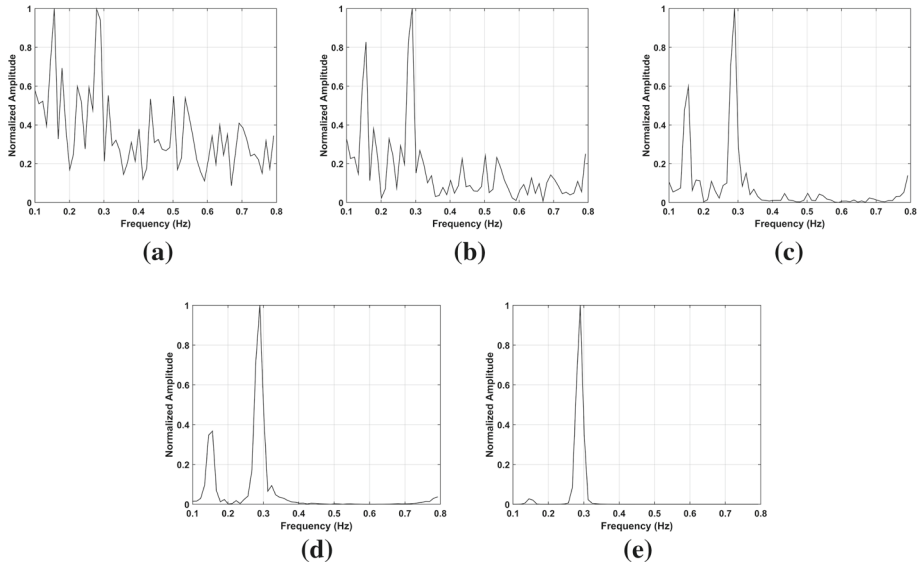
Fig. 16 The spectrums using **a** FFT, **b** one FA, **c** two FA, **d** three FA, and **e** four FA

6 Conclusion

In this paper, a new method for vital sign feature (VSF) detection is presented using the UWB pulse radar. The time of arrival (TOA) of the UWB pulse reflected by human beings can be estimated by employing the discrete windowed Fourier transform (DWFT) on the skewness and standard deviation of the received signal. The accumulation method in frequency domain is developed to cancel out the mixed products and harmonics of life signal. The presented

Table 3 Performance on improving SNR

Method	FFT	One FA	Two FA	Three FA	The new
SNR (dB)	− 8.37	− 5.49	− 3.26	− 2.73	2.17

algorithm provides a preliminary signature for the search and rescue of victims in nature disaster. Experimental results in different conditions show the better capability of removing clutter and improving SNR.

References

Allen, B. (1977). Short term spectral analysis, synthesis, and modification by discrete fourier transform. *IEEE Transactions on Acoustics, Speech, and Signal Processing, 25*(3), 235–238.

Ascione, M., et al. (2013). A new measurement method based on music algorithm for through-the-wall detection of life signs. *IEEE Transactions on Instrumentation and Measurement, 62*(1), 13–26.

Baldi, M., et al. (2015). Non-invasive UWB sensing of astronauts' breathing activity. *Sensors, 15*(1), 565–591.

Conte, E., Filippi, A., & Tomasin, S. (2010). ML period estimation with application to vital sign monitoring. *IEEE Signal Processing Letters, 17*(11), 905–908.

Gennarelli, G., Ludeno, G., & Soldovieri, F. (2016). Real-time through-wall situation awareness using a microwave doppler radar sensor. *Remote Sensing, 8*(8), 621.

Gu, C., & Li, C. (2015). Assessment of human respiration patterns via noncontact sensing using doppler multi-radar system. *Sensors, 15*(3), 6383–6398.

Hu, X., & Jin, T. (2016). Short-range vital signs sensing based on EEMD and CWT using IR-UWB radar. *Sensors, 16*(12), 2025.

Hu, W., et al. (2014). Noncontact accurate measurement of cardiopulmonary activity using a compact quadrature Doppler radar sensor. *IEEE Transactions on Biomedical Engineering, 61*(3), 725–735.

Huang, Q., Qu, L., & Fang, G. (2010). UWB through-tall imaging based on compressive sensing. *IEEE Transactions on Geoscience and Remote Sensing, 48*(3), 1408–1415.

Huang, M. C., et al. (2016). A self-calibrating radar sensor system for measuring vital signs. *IEEE Transactions on Biomedical Circuits and Systems, 10*(2), 352–363.

JalaliBidgoli, F., Moghadami, S., & Ardalan, S. (2016). A compact portable microwave life-detection device for finding survivors. *IEEE Embedded Systems Letters, 8*(1), 10–13.

Koo, Y. S., et al. (2013). UWB MicroDoppler radar for human gait analysis, tracking more than one person, and vital sign detection of moving persons. In *IEEE MTT-S International Microwave Symposium Digest, Seattle, WA, USA* (pp. 1–4).

Lazaro, A., Girbau, D., & Villarino, R. (2014). Techniques for clutter suppression in the presence of body movements during the detection of respiratory activity through UWB radars. *Sensors, 14*(2), 2595–2618.

Le, C., et al. (2009). Ultra-wideband radar imaging of building interior: Measurements and predictions. *IEEE Transactions on Geoscience and Remote Sensing, 47*(5), 1409–1420.

Li, W. Z. (2013). A new method for non-line-of-sight vital sign monitoring based on developed adaptive line enhancer using low centre frequency UWB radar. *Progress in Electromagnetics Research, 133*(34), 535–554.

Li, C., & Lin, J. (2008). Random body movement cancellation in Doppler radar vital sign detection. *IEEE Transactions on Microwave Theory and Techniques, 56*(12), 3143–3152.

Li, Z., et al. (2013). A novel method for respiration-like clutter cancellation in life detection by dual-frequency IR-UWB radar. *IEEE Transactions on Microwave Theory and Techniques, 61*(5), 2086–2092.

Li, J., et al. (2014). Advanced signal processing for vital sign extraction with applications in UWB radar detection of trapped victims in complex environments. *IEEE Journal of Selected Topics in Applied Earth Observations and Remote Sensing, 7*(3), 783–791.

Liang, S. D. (2016). Sense-through-wall human detection based on UWB radar sensors. *Signal Process, 126*, 117–124.

Liang, X., et al. (2017). Energy detector based TOA estimation for MMW systems using machine learning. *Telecommunication Systems, 64*(2), 417–427.

Liang, X., et al. (2018a). Experimental study of wireless monitoring of human respiratory movements using UWB impulse radar systems. *Sensors, 18*(9), 3065.

Liang, X., et al. (2018b). Ultra-wideband impulse radar through-wall detection of vital signs. *Scientific Reports, 8,* 13367.

Liang, X., et al. (2018c). An improved algorithm for through-wall target detection using ultra-wideband impulse radar. *IEEE Access, 5*(99), 22101–22118.

Liang, X., et al. (2018d). Improved denoising method for through-wall vital sign detection using UWB impulse radar. *Digital Signal Processing, 74,* 72–93.

Liang, X., et al. (2018e). Ultra-wide band impulse radar for life detection using wavelet packet decomposition. *Physical Communication, 4*(4), 1–20.

Liang, X., et al. (2018f). Through-wall human being detection using UWB impulse radar. *EURASIP Journal on Wireless Communications and Networking, 2018*(46), 1–17.

Liu, L., Liu, Z., & Barrowes, B. (2011). Through-wall bio-radiolocation with UWB impulse radar—Observation, simulation and signal extraction. *IEEE Journal of Selected Topics in Applied Earth Observations and Remote Sensing, 4*(4), 791–798.

Liu, L., et al. (2014). Numerical simulation of UWB impulse radar vital sign detection at an earthquake disaster site. *Ad Hoc Networks, 13*(1), 34–41.

Lv, H., et al. (2016). Improved detection of human respiration using data fusion based on a multistatic UWB radar. *Remote Sensing, 8*(9), 773.

Mak, J. C. C., Bois, A., & Poon, J. K. S. (2016). Programmable multiring butterworth filters with automated resonance and coupling tuning. *IEEE Journal of Selected Topics in Quantum Electronics, 22*(6), 1–9.

Marple, L. (1999). Computing the discrete-time "analytic" signal via FFT. *IEEE Transactions on Signal Processing, 47*(9), 2600–2603.

Mercuri, M., et al. (2013). Optimized SFCW radar sensor aiming at fall detection in a real room environment. In *Proceedings of the IEEE biomedical wireless technologies, networks, and sensing systems*, Austin, TX, USA (pp. 4–6).

Mercuri, M., et al. (2013). Analysis of an indoor biomedical radar-based system for health monitoring. *IEEE Transactions on Microwave Theory and Techniques, 61*(5), 2061–2068.

Naishadham, K., & Piou, J. E. (2008). A robust state space model for the characterization of extended returns in radar target signatures. *IEEE Transactions on Antennas and Propagation, 56*(6), 1742–1751.

Nezirovíc, A., Yarovoy, A., & Ligthart, L. (2010). Signal processing for improved detection of trapped victims using UWB radar. *IEEE Transactions on Geoscience and Remote Sensing, 48*(4), 2005–2014.

Nijsure, Y., et al. (2013). An impulse radio ultrawideband system for contactless noninvasive respiratory monitoring. *IEEE Transactions on Biomedical Engineering, 60*(6), 1509–1517.

Park, B. K., Boric-Lubecke, O., & Lubecke, V. M. (2007). Arctangent demodulation with DC offset compensation in quadrature Doppler radar receiver systems. *IEEE Transactions on Microwave Theory and Techniques, 55*(5), 1073–1079.

Ren, L. (2015). Noncontact multiple heartbeats detection and subject localization using UWB impulse doppler radar. *IEEE Microwave and Wireless Components Letters, 25*(10), 690–692.

Ren, L., et al. (2016). Phase-based methods for heart rate detection using UWB impulse Doppler radar. *IEEE Transactions on Microwave Theory and Techniques, 64*(10), 3319–3331.

Singh, A., et al. (2013). Data-based quadrature imbalance compensation for a CW Doppler radar system. *IEEE Transactions on Microwave Theory and Techniques, 61*(4), 1718–1724.

Vu, V. T., et al. (2010). Detection of moving targets by focusing in UWB SAR theory and experimental results. *IEEE Transactions on Geoscience and Remote Sensing, 48*(10), 3799–3815.

Wang, S., et al. (2015). A novel ultra-wideband 80 GHz FMCW radar system for contactless monitoring of vital signs. In *Proceedings of the IEEE engineering in medicine and biology society*, Milan, Italy (pp. 4978–4981).

Wang, Y., Liu, Q., & Fathy, A. E. (2012). Simultaneous localization and respiration detection of multiple people using low cost UWB biometric pulse Doppler radar sensor. In *IEEE MTT-S* international *microwave symposium digest, Montreal, QC, Canada* (pp. 1–3).

Wang, Y., Liu, Q., & Fathy, A. E. (2013). CW and pulse-Doppler radar processing based on FPGA for human sensing applications. *IEEE Transactions on Geoscience and Remote Sensing, 51*(5), 3097–3107.

Wang, J., et al. (2014a). Noncontact distance and amplitude-independent vibration measurement based on an extended DACM algorithm. *IEEE Transactions on Instrumentation and Measurement, 63*(1), 145–153.

Wang, G., et al. (2014b). A hybrid FMCW-interferometry radar for indoor precise positioning and versatile life activity monitoring. *IEEE Transactions on Microwave Theory and Techniques, 62*(11), 2812–2822.

Wang, Z., et al. (2018a). Cooperative RSS-based localization in wireless sensor networks using relative error estimation and semidefinite programming. *IEEE Transactions on Vehicular Technology*. https://doi.org/10.1109/TVT.2018.2880991.

Wang, Z., et al. (2018b). A grid-based localization algorithm for wireless sensor networks using connectivity and RSS rank. *IEEE Access, 6*(1), 8426–8439.

Wójcicki, K., et al. (2008). Exploiting conjugate symmetry of the short-time Fourier spectrum for speech enhancement. *IEEE Signal Processing Letters, 15,* 461–464.

Wu, S., et al. (2016). Improved human respiration detection method via ultra-wideband radar in through-wall or other similar conditions. *IET Radar, Sonar and Navigation, 10*(3), 468–476.

Zhang, Z. (2013). Human-target detection and surrounding structure estimation under a simulated rubble via UWB radar. *IEEE Transactions on Geoscience and Remote Sensing, 10*(2), 328–331.

Zhuge, X., & Yarovoy, A. (2011). A sparse aperture MIMO-SAR based UWB imaging system for concealed weapon detection. *IEEE Transactions on Geoscience and Remote Sensing, 49*(1), 509–518.